# Fine-structure resolved rovibrational transitions for SO + H<sub>2</sub> collisions

Cite as: J. Chem. Phys. **154**, 034301 (2021); https://doi.org/10.1063/5.0036964 Submitted: 11 November 2020 . Accepted: 23 December 2020 . Published Online: 15 January 2021

🗓 Teri J. Price, 🗓 Robert C. Forrey, 🗓 Benhui Yang, and 🗓 Phillip C. Stancil

#### **COLLECTIONS**

Paper published as part of the special topic on Special Collection in Honor of Women in Chemical Physics and Physical Chemistry







#### ARTICLES YOU MAY BE INTERESTED IN

Collisional excitation of interstellar PN by H<sub>2</sub>: New interaction potential and scattering calculations

The Journal of Chemical Physics 154, 034304 (2021); https://doi.org/10.1063/5.0039145

Accurate DMBE potential-energy surface for  $CNO(^2A'')$  and rate coefficients in  $C(^3P)+NO$  collisions

The Journal of Chemical Physics 154, 034303 (2021); https://doi.org/10.1063/5.0031199

Time resolved detection of the S(<sup>1</sup>D) product of the UV induced dissociation of CS<sub>2</sub>
The Journal of Chemical Physics 154, 034302 (2021); https://doi.org/10.1063/5.0035045





## Fine-structure resolved rovibrational transitions for SO + H<sub>2</sub> collisions

Cite as: J. Chem. Phys. 154, 034301 (2021); doi: 10.1063/5.0036964 Submitted: 11 November 2020 • Accepted: 23 December 2020 • Published Online: 15 January 2021











Teri J. Price, De Robert C. Forrey, Benhui Yang, De and Phillip C. Stancil



#### **AFFILIATIONS**

- Department of Physics, Penn State University, Berks Campus, Reading, Pennsylvania 19610-6009, USA
- <sup>2</sup>Department of Physics and Astronomy and the Center for Simulational Physics, University of Georgia, Athens, Georgia 30602, USA

Note: This paper is part of the JCP Special Collection in Honor of Women in Chemical Physics and Physical Chemistry.

<sup>a)</sup>Author to whom correspondence should be addressed: rcf6@psu.edu

#### **ABSTRACT**

Cross sections and rate coefficients for sulfur monoxide (SO) + H<sub>2</sub> collisions are calculated using a full six-dimensional (6D) potential energy surface (PES). The coupled states (CS) approximation is used to compute fine-structure resolved cross sections for rovibrational transitions between states with v = 0-2, where v is the vibrational quantum number of the SO molecule. The CS calculations for  $\Delta v = 1$  are benchmarked against close-coupling (CC) results for spin-free interactions. For  $\Delta v = 0$ , the present fine-structure resolved CS results are benchmarked against existing CC results obtained with a rigid rotor approximation. In both cases, the agreement is found to be satisfactory, which suggests that the present results may provide reliable estimates for fine-structure resolved rovibrational transitions. These estimates are the first of their kind based on a full 6D PES. Rate coefficients are reported for temperatures between 10 K and 3000 K for both para- and ortho-H<sub>2</sub> colliders. A comparison of the para-H<sub>2</sub> rates with mass-scaled results for He shows substantial differences that may be important in astrophysical

Published under license by AIP Publishing. https://doi.org/10.1063/5.0036964

#### I. INTRODUCTION

Sulfur monoxide (SO) was first observed in the interstellar medium by Gottlieb and Ball<sup>1</sup> in the early 1970s. It is a tracer of shock regions and regions of hot dense gas,<sup>2</sup> and it has been observed in a variety of astrophysical environments, including dark, diffuse, and dense molecular clouds<sup>3-6</sup> in low- and high-mass star-forming regions,<sup>2,7</sup> circumstellar envelopes,<sup>8</sup> massive dense cores,<sup>9</sup> and protoplanetary disks.  $^{10,11}$  A molecule with a  $^3\Sigma$  ground state, SO has relatively closely spaced fine structure levels that make it a useful probe of the physical and chemical composition of its environment. In non-local thermodynamic equilibrium (non-LTE) environments, a large database of state-resolved rate coefficients is often required to obtain reliable estimates of molecular column densities and kinetic temperatures. Due to the difficulty in measuring large amounts of state-to-state collision data, astrophysical models generally rely on theoretical calculations of collisional cross sections to obtain the needed rate coefficients. 12

Fine-structure resolved transitions for SO  $(X^3\Sigma^-)$  induced by collisions with H<sub>2</sub> have been calculated by Green<sup>16</sup> and Lique et al.; <sup>1</sup> both are available in the BASECOL database. 18 Green 16 calculated fine-structure resolved rotational transitions between rigid rotator SO and para-H<sub>2</sub> for temperatures ranging from 50 K to 350 K. The dynamical calculations utilized the CS approximation to determine spin-free T-matrices, which were recoupled using infiniteorder sudden (IOS) scaling relationships. For these calculations, Green used a PES for CS-H<sub>2</sub> and the reduced mass for SO-H<sub>2</sub>.

Lique et al. 17 calculated fine-structure resolved rotational transitions between rigid rotator SO and para-H2 for temperatures up to 50 K. They used the CC formalism along with a 4D PES for SO-H<sub>2</sub>; the PES was reduced to a 2D potential by averaging over the angular degrees of freedom for H<sub>2</sub>, approximating it as a structureless particle. Due to the large spin-rotation coupling constant for SO  $(X^3\Sigma^-)$ , Lique et al. 17 used an intermediate coupling scheme between Hund's cases (a) and (b) to determine fine-structure transitions. In a related work, Lique et al. 19 performed calculations for rovibrational excitation of SO in collision with He using the vibrational close-coupling rotational IOS approximation for temperatures from 300 K to 800 K. The calculation of vibrational de-excitation rate coefficients of SO from the first two vibrational levels was reported, and the results have been mass-scaled to obtain rough estimates for para-H<sub>2</sub> colliders. Lique *et al.* also computed rotational SO–He data<sup>20,21</sup> using the rigid rotator approximation. Their excitation rate coefficients were used in models of the physical conditions in the TMC-1 molecular cloud.<sup>22</sup>

The present work extends these previous calculations of finestructure resolved transitions by including both para- and ortho-H<sub>2</sub> perturbers over collision energies between 10 cm<sup>-1</sup> and 10 000 cm<sup>-1</sup> and uses a new and improved PES.<sup>23</sup> The basis set includes higher vibrational levels of SO and the first excited rotational level for each symmetry of H<sub>2</sub>. The dynamical calculations are performed within the 5D-CS approximation,<sup>24</sup> and fine-structure resolved cross sections are determined by recoupling the spin-free T-matrices. The differences between the 5D-CS and 6D-CC cross sections are similar to those seen for CO-H<sub>2</sub>, <sup>24</sup> SiO-H<sub>2</sub>, <sup>25</sup> and CN-H<sub>2</sub>. <sup>26</sup> The spin-free results compare favorably with the exact 6D-CC results for v = 0 and 1 reported by Yang et al.<sup>23</sup> and provide a measure of accuracy for the 5D-CS approximation for transitions involving large j or v for which the CC calculations become intractable. Transitions between fine-structure levels of SO are also compared with those calculated by Lique et al. 17,19 Significant differences are seen for vibrational deexcitation, where the present results should be more reliable than mass-scaled results for SO colliding with He.19

This paper is organized as follows. The theory is outlined in Sec. II. Spin-free and fine-structure resolved results are presented and compared with other available calculations in Secs. III A and III B, respectively. A summary of the results and conclusions is given in Sec. IV.

#### II. THEORY

This work utilizes the 6D-PES presented by Yang *et al.*<sup>23</sup> The PES is described in terms of the 6D Jacobi coordinate system shown in Fig. 1. In this coordinate system, R is the distance between the center-of-masses of the diatomic molecules,  $\theta_1$  is the angle between  $\vec{r}_1$  and  $\vec{R}$ ,  $\theta_2$  is the angle between  $\vec{r}_2$  and  $\vec{R}$ , and  $\phi$  is the out-of-plane dihedral or "twist" angle between the two molecules. The 5D-CS approximation assumes a weak dependence on the twist angle

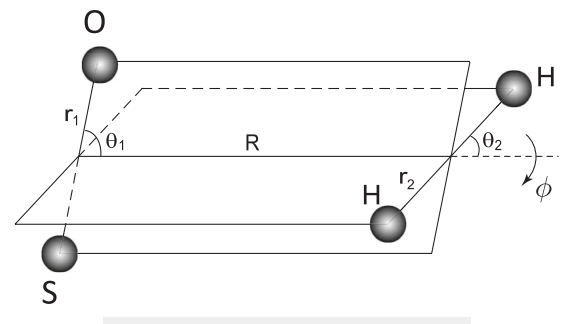


FIG. 1. Jacobi coordinate system for SO-H<sub>2</sub>.

 $\phi$  and averages over this degree of freedom.<sup>24</sup> This approximation is justified by the 6D-PES, <sup>23</sup> which exhibits a weak  $\phi$  dependence; the dependence becomes increasingly weak as R increases. Figure 2 shows a representative plot for a specific configuration.

To describe the dynamics, we start by neglecting spin and focus on the combined molecular state (CMS) comprised of  $SO(v_1, j_1)$  and  $H_2(v_2, j_2)$  using the notation  $n = (v_1, j_1, v_2, j_2)$ . The Hamiltonian of the diatom–diatom system is given by

$$H(\vec{r}_1, \vec{r}_2, \vec{R}) = T(\vec{r}_1) + T(\vec{r}_2) + T(\vec{R}) + V(\vec{r}_1, \vec{r}_2, \vec{R}). \tag{1}$$

The radial kinetic energy term  $T(\vec{R})$  describes the center-of-mass motion, and the terms  $T(\vec{r}_1)$  and  $T(\vec{r}_2)$  represent the kinetic energies of the SO and H<sub>2</sub> molecules, respectively. The potential energy for the diatom–diatom system is given by

$$V(\vec{r}_1, \vec{r}_2, \vec{R}) = U(\vec{r}_1, \vec{r}_2, \vec{R}) + V(\vec{r}_1) + V(\vec{r}_2), \tag{2}$$

where  $V(\vec{r}_1)$  and  $V(\vec{r}_2)$  are the potential energies of the isolated SO and  $H_2$  molecules and  $U(\vec{r}_1,\vec{r}_2,\vec{R})$  is the diatom–diatom interaction potential that vanishes at large separations. The interaction potential may be expanded as

$$U(\vec{r}_1, \vec{r}_2, \vec{R}) = \sum_{\lambda_1, \lambda_2, \lambda_{12}} A_{\lambda_1, \lambda_2, \lambda_{12}}(r_1, r_2, R) Y_{\lambda_1, \lambda_2, \lambda_{12}}(\hat{r}_1, \hat{r}_2, \hat{R}), \quad (3)$$

with

$$Y_{\lambda_{1},\lambda_{2},\lambda_{12}}(\hat{r}_{1},\hat{r}_{2},\hat{R}) = \sum_{\text{all }m} \langle \lambda_{1} m_{\lambda_{1}} \lambda_{2} m_{\lambda_{2}} | \lambda_{12} m_{\lambda_{12}} \rangle$$

$$\times Y_{\lambda_{1} m_{\lambda_{1}}}(\hat{r}_{1}) Y_{\lambda_{2} m_{\lambda_{2}}}(\hat{r}_{2}) Y_{\lambda_{12} m_{\lambda_{12}}}^{*}(\hat{R}), \qquad (4)$$

where  $\langle \cdots | \cdots \rangle$  represents a Clebsch–Gordan coefficient and  $Y_{\lambda m}(\hat{r})$  is a spherical harmonic. The total wave function for the diatom–diatom system is expanded in terms of a diabatic basis set, which contains products of molecular wave functions  $\chi_{v_{ij_i}}(r_i)$  with vibrational and rotational quantum numbers  $v_i$  and  $j_i$ , respectively. Using

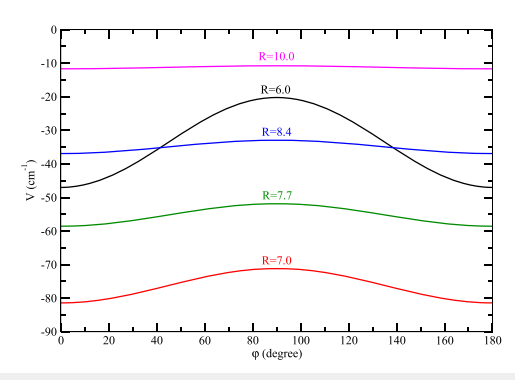


**FIG. 2.** Potential energy as a function of twist angle  $\phi$  for different intermolecular separations R, with  $\theta_1 = \theta_2 = 90^\circ$ , and each molecule near its equilibrium separation. The dependence on the twist angle becomes increasingly weak as R increases. The minimum of the PES is at R = 7.7  $a_0$  with  $\theta_1 = \theta_2 = 0^\circ$ ; the most significant twist angle dependence arises near the repulsive wall of the PES.

the additional notations  $v \equiv v_1$ ,  $v_2$  and  $j \equiv j_1$ ,  $j_2$ , the radial interaction potential matrix elements are obtained by integrating over the internal coordinates

$$B_{\nu_{j},\nu'j'}^{\lambda_{1},\lambda_{2},\lambda_{12}} = \left\langle \chi_{\nu_{1}j_{1}} \chi_{\nu_{2}j_{2}} | A_{\lambda_{1},\lambda_{2},\lambda_{12}} | \chi_{\nu'_{1}j'_{1}} \chi_{\nu'_{2}j'_{2}} \right\rangle. \tag{5}$$

The full potential matrix within the 5D-CS calculations has been described previously<sup>24</sup> and is independent of  $j_{12}$  and diagonal with respect to  $m_1$  and  $m_2$ , the projection quantum numbers of  $\vec{j}_1$  and  $\vec{j}_2$ . The set of coupled equations of the form

$$\left[ -\frac{\hbar^2}{2\mu} \frac{d^2}{dR^2} + \frac{\hbar^2 l(l+1)}{2\mu R^2} - E_c \right] F_n(R) + \sum_{n'} V_{n;n'}(R) F_{n'}(R) = 0 \quad (6)$$

is solved, where  $E_c = E - E_n$  is the relative collision energy in the incident channel. The CS approximation neglects the off-diagonal elements of  $\hat{l}^2$  with respect to  $\Omega$ , the projection of  $\vec{J}$  onto the body-fixed z axis, and it approximates the diagonal elements by an effective orbital angular momentum quantum number  $\bar{l}$ , which replaces l in Eq. (6). In this work,  $\bar{l} \equiv J$  is the average value of l between  $|J - j_{12}|$  and  $J + j_{12}$ . The spin-free 5D-CS cross sections at a given collision energy  $E_c$  and wave number  $k_n$  may be expressed in terms of the T-matrix by

$$\sigma_{n \to n'}^{\text{5D-CS}} = \frac{\pi}{k_n^2} \left[ (2j_1 + 1)(2j_2 + 1) \right]^{-1} \sum_{\bar{l}m_1m_2} (2\bar{l} + 1) \left| T_{n;n'}^{\bar{l}m_1m_2} \right|^2. \tag{7}$$

We account for the spin-rotation coupling of SO( $X^3\Sigma^-$ ) by recoupling the spin-free results. 
<sup>27–29</sup> For rotational energy spacings that are not too small, SO( $X^3\Sigma^-$ ) follows a pure Hund's case (b) coupling scheme. The CMS for SO + H<sub>2</sub> in this case becomes  $n=(v_1, N_1, j_1, v_2, j_2)$ , where  $\vec{j}_1 = \vec{N}_1 + \vec{S}_1$  and  $\vec{S}_1$  is the total electronic spin of SO. Within the 5D-CS approximation, the fine-structure resolved cross sections are given by <sup>26</sup>

$$\sigma_{n \to n'}^{5D-CS} = \frac{\pi}{k_n^2} \sum_{\tilde{l}m_1 m_2 \mu_1} \frac{(2\tilde{l}+1)}{(2j_1+1)(2j_2+1)} T_{n,n'}^{\tilde{l}m_1 m_2} T_{n,n'}^{\tilde{l}m'_1 m_2}$$

$$\times \begin{pmatrix} S_1 & N_1 & j_1 \\ -m'_1 - \mu_1 & m'_1 & \mu_1 \end{pmatrix} \begin{pmatrix} S_1 & N_1 & j_1 \\ -m_1 - \mu_1 & m_1 & \mu_1 \end{pmatrix}$$

$$\times \begin{pmatrix} S_1 & N'_1 & j'_1 \\ -m'_1 - \mu_1 & m'_1 & \mu_1 \end{pmatrix} \begin{pmatrix} S_1 & N'_1 & j'_1 \\ -m_1 - \mu_1 & m_1 & \mu_1 \end{pmatrix}, \quad (8)$$

where  $m_1$  and  $\mu_1$  are the projection quantum numbers of  $N_1$  and  $j_1$ , respectively, and  $(\cdots)$  is a Wigner 3j symbol. It should be noted that the T-matrix elements were calculated without incorporating the energy splitting of the fine structure levels. These splittings are

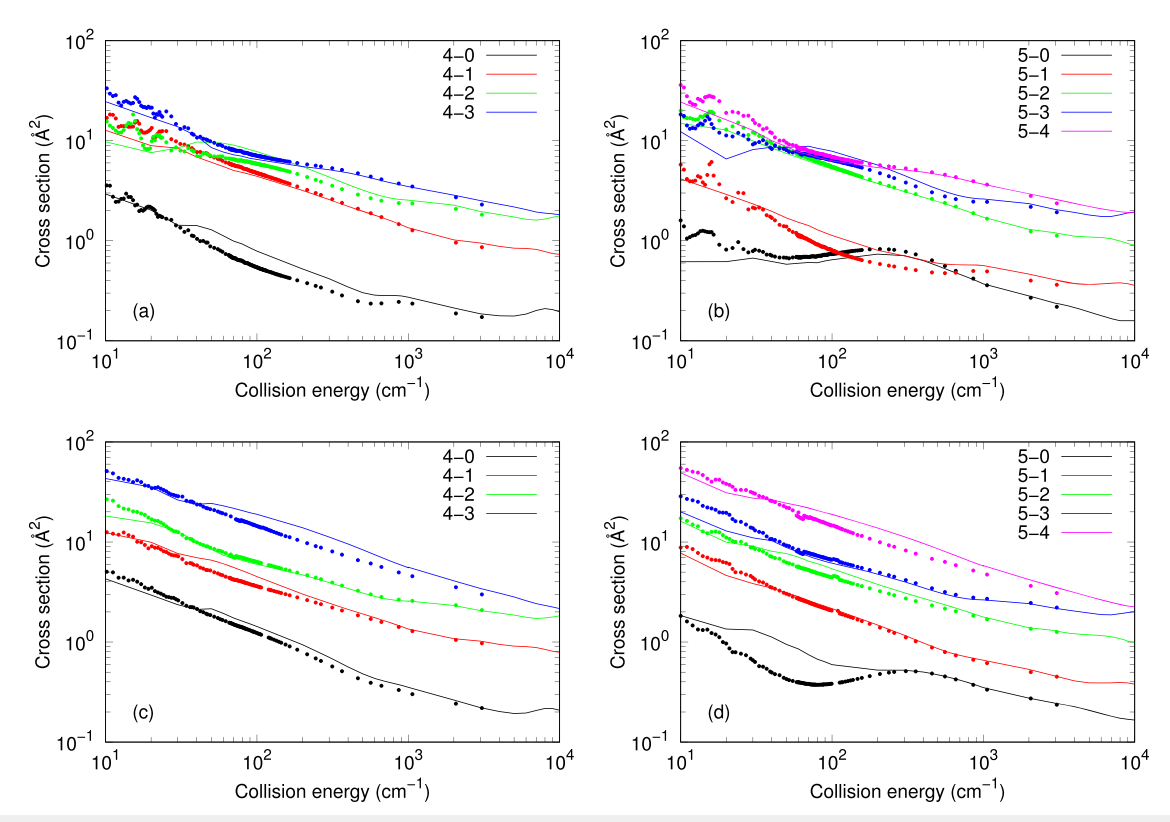


**FIG. 3**. Comparison between 6D-CC (points) and 5D-CS (solid lines) rotational de-excitation cross sections for v = 0. Panels (a) and (b) show results for collisions between SO and para-H<sub>2</sub> for initial states  $j_1 = 4$  and 5, respectively. Panels (c) and (d) show a similar comparison but for SO + ortho-H<sub>2</sub>. The key labels the transitions as  $j_1 - j_1'$ , where  $j_1'$  is the final rotational level of SO.

expected to have a negligible effect at the temperatures of interest, so considerable computational time is saved by not enlarging the set of coupled equations.

The spin-rotation coupling constant for  $SO(X^3\Sigma^-)$  is larger than the rotation constant, so for low  $N_1$  values, the recoupling should be done with a scheme that is intermediate between Hund's cases (a) and (b). We follow the work of Lique *et al.*<sup>17</sup> and use the method described by Corey, Alexander, and Schaefer<sup>30</sup> to define the states in the intermediate coupling case  $(F_1, F_2, F_3)$  in terms of the Hund's case (b) basis states,

$$|F_{1}j_{1}m_{1}\rangle = \cos \alpha |(N_{1} = j_{1} - 1, S_{1})j_{1}m_{1}\rangle + \sin \alpha |(N_{1} = j_{1} + 1, S_{1})j_{1}m_{1}\rangle, |F_{2}j_{1}m_{1}\rangle = |(N_{1}, S_{1})j_{1}m_{1}\rangle, |F_{3}j_{1}m_{1}\rangle = -\sin \alpha |(N_{1} = j_{1} - 1, S_{1})j_{1}m_{1}\rangle + \cos \alpha |(N_{1} = j_{1} + 1, S_{1})j_{1}m_{1}\rangle.$$
(9)

As outlined in the Appendix, we compute the mixing angle  $\alpha$  by diagonalizing the SO Hamiltonian in the Hund's case (b) basis set, using the experimental spectroscopic constants from the work of Bogey *et al.*<sup>31</sup> This leads to the desired cross section,

$$\sigma_{F,j\to F',j'}^{\text{5D-CS}} = \frac{\pi}{k_n^2} \sum_{\bar{l}m_1m_2\mu_1} \frac{(2\bar{l}+1)}{(2j_1+1)(2j_2+1)} \times \sum_{N_1N_1'N_1''N_1'''} C_{N_1F_i}^{j_1} C_{N_1'F_i}^{j_1} C_{N_1''F_i'}^{j_1} \times C_{N_1'''F_i'}^{j_1} T_{N_1;N_1''}^{\bar{l}m_1m_2} T_{N_1';N_1'''}^{*\bar{l}m_1'm_2} \times \begin{pmatrix} S_1 & N_1 & j_1 \\ -m_1 - \mu_1 & m_1 & \mu_1 \end{pmatrix} \begin{pmatrix} S_1 & N_1' & j_1 \\ -m_1' - \mu_1 & m_1' & \mu_1 \end{pmatrix} \times \begin{pmatrix} S_1 & N_1'' & j_1 \\ -m_1 - \mu_1 & m_1 & \mu_1 \end{pmatrix} \begin{pmatrix} S_1 & N_1'' & j_1 \\ -m_1' - \mu_1 & m_1' & \mu_1 \end{pmatrix}, \quad (10)$$

where  $C_{N_1F_i}^{f_1}$  are the coefficients of the Hund's case (b) basis states in Eq. (9).

Rate coefficients at a temperature T may be obtained for all coupling schemes by thermally averaging the cross sections over a Maxwellian velocity distribution,

$$q_{n \to n'}(T) = \sqrt{\frac{8k_{\rm B}T}{\pi \mu}} (k_{\rm B}T)^{-2} \int_0^\infty \sigma_{n \to n'}(E_{\rm c}) e^{-E_{\rm c}/k_{\rm B}T} E_{\rm c} dE_{\rm c}, \quad (11)$$

where  $\mu$  is the reduced mass of the SO + H<sub>2</sub> system and  $k_{\rm B}$  is Boltzmann's constant.

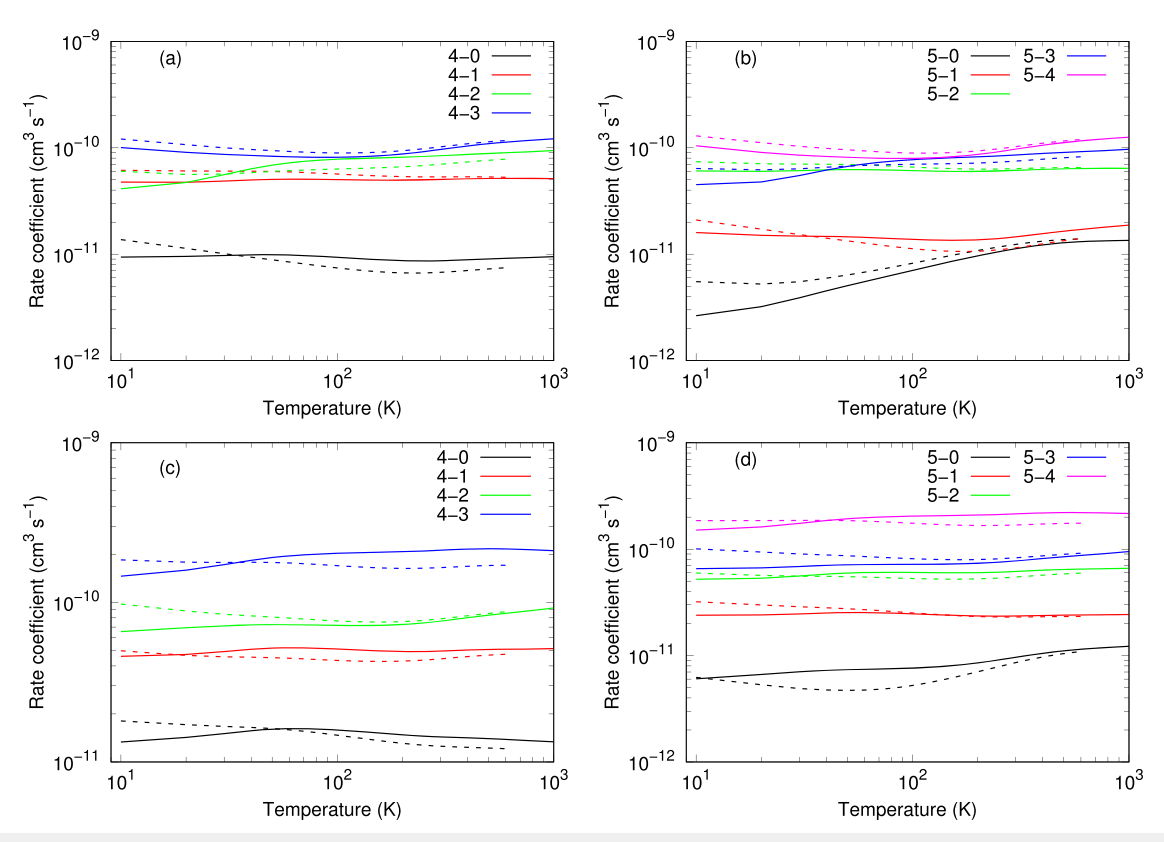


**FIG. 4.** Comparison between 6D-CC (dashed lines) and 5D-CS (solid lines) rotational de-excitation rate coefficients for v = 0. Panels (a) and (b) show results for collisions between SO and para-H<sub>2</sub> for initial states  $j_1 = 4$  and 5, respectively. Panels (c) and (d) show a similar comparison but for SO + ortho-H<sub>2</sub>. The key labels the transitions as  $j_1 - j_1^2$ , where  $j_1^2$  is the final rotational level of SO.

#### III. RESULTS

All calculations were performed using the 6D PES reported previously by Yang et al.<sup>23</sup> and accurate diatomic potentials.<sup>32</sup> scattering calculations were performed using a modified version of the TwoBC code,<sup>34</sup> which replaces the 6D-CC formulation by the 5D-CS approximation. The radial coordinates of both molecules were represented as discrete variables with 18 points each. Gauss-Legendre quadratures were used for  $\theta_1$  and  $\theta_2$  with 12 points each. The maximum values for  $\lambda_1$  and  $\lambda_2$  were 8 and 4, respectively. The log-derivative matrix propagation method<sup>35,36</sup> was used to integrate the set of coupled equations derived from the Schrödinger equation for  $R = 4.5-25 \ a_0$  in steps of 0.05  $a_0$ , where  $a_0 = 0.529 \ \text{Å}$  is the Bohr radius. The parameters given above are identical to those used previously,<sup>23</sup> which enables a controlled comparison with the 6D-CC results. The calculations were performed in unit steps on a logarithmic energy grid for four sets of collision energies ranging from 1 cm<sup>-1</sup> to 10 000 cm<sup>-1</sup>; the sets included 20, 40, 80, and 160 partial waves, respectively. The basis set for the SO molecule included  $j_1 = 0-40$  for  $v_1 = 0$  and 1 and  $j_1 = 0-20$  for  $v_1 = 2$ . The basis set for H<sub>2</sub> allowed for rotational excitation to the first excited rotational level for each symmetry ( $j_2 = 0$ , 2 for para- $H_2$  and  $j_2 = 1$ , 3 for ortho- $H_2$ ) with  $v_2 = 0$ .

In Secs. III A and III B, 5D-CS calculations for SO-H<sub>2</sub> are compared with available results. In Sec. III A, spin-free results are compared with those reported by Yang *et al.*, <sup>23</sup> which were obtained by using the numerically exact 6D-CC formalism. In Sec. III B, fine-structure resolved cross sections for rotational transitions are compared with those calculated by Lique *et al.* <sup>17</sup> We also compare fine-structure resolved rovibrational cross sections to the mass-scaled SO-He results of Lique *et al.* <sup>19</sup> A comparison with He collisional data is not expected to be quantitative; however, it helps to illustrate the importance of rigorous calculations.

#### A. Spin-free results

To assess the reliability of the spin-free CS calculations, we first benchmark the 5D-CS results against numerically exact 6D-CC results. Figure 3 compares selected rotational de-excitation cross sections for SO due to collisions with  $H_2$ . Panels (a) and (b) show results with para- $H_2(0,0)$  as the perturber, and panels (c) and (d) show results with ortho- $H_2(0,1)$  as the collider. For both collision partners, the 5D-CS and 6D-CC results agree qualitatively, with the CS approximation, reproducing the main features of the CC cross sections. As the collision energy increases, the quantitative agreement improves, with the cross sections generally within less

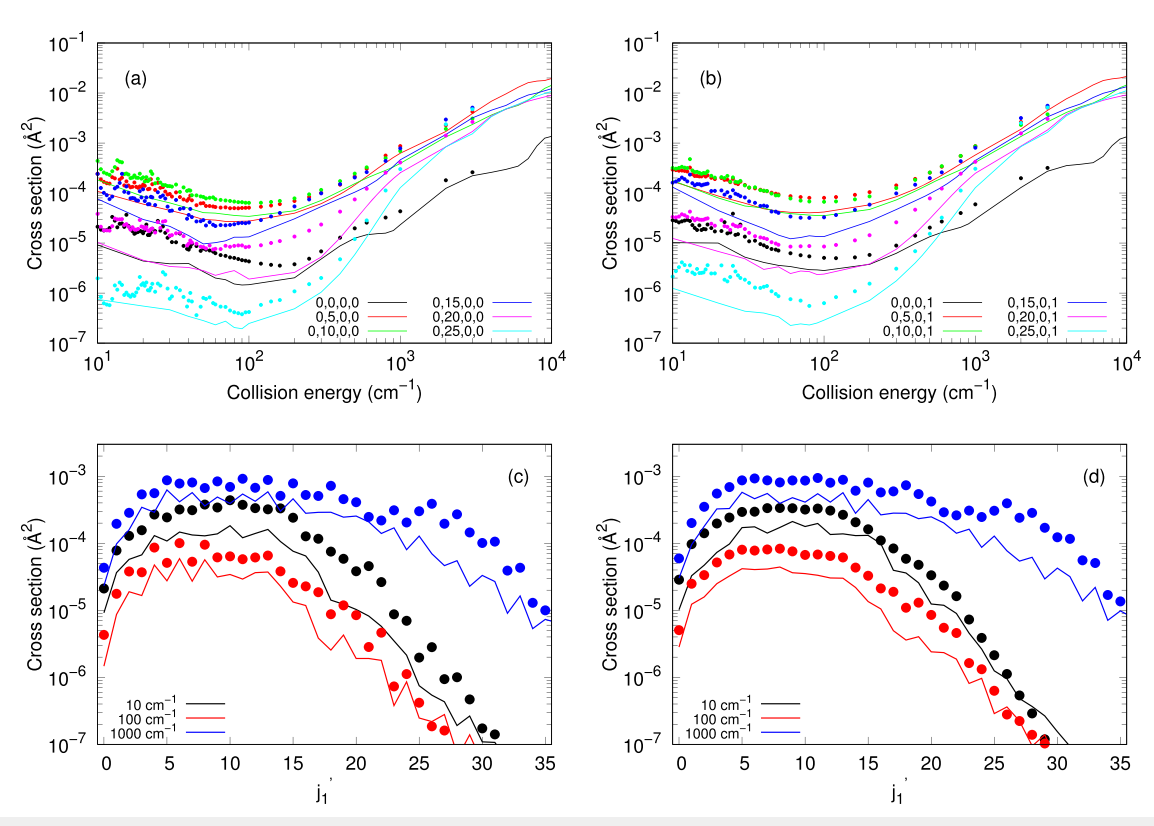


**FIG. 5.** Comparison between 6D-CC (points) and 5D-CS (solid lines) vibrational de-excitation cross sections. Panel (a) shows results for collisions between SO(1,5) and para- $H_2$  as a function of energy for six different final states labeled  $v_1$ ,  $j_1$ ,  $v_2$ ,  $j_2$ . Panel (b) is similar to panel (a) but with ortho- $H_2$  as the perturber. Panel (c) shows cross sections from SO(1,5) to SO(0,  $j_1'$ ) induced by collisions with para- $H_2$  for three different collision energies. Panel (d) is similar to panel (c) but with ortho- $H_2$  as the perturber.

than 30% for  $E_c > 100 \text{ cm}^{-1}$ . When para-H<sub>2</sub> collides with SO, the dominant cross sections reveal a competition between transitions that minimize the internal energy and angular momentum gaps (i.e.,  $\Delta j_1 = -1$ ) and ones with  $\Delta j_2 = -2$ . This tendency for the latter behavior arises because the interaction potential is approximately symmetric under the interchange of the S and O atoms, which

suppresses odd  $\Delta j$ , as has been observed in other systems of similar symmetry. This behavior is reduced for ortho- $H_2$  colliders as the cross sections appear to be more evenly spaced. Resonances are clearly seen in the 6D-CC cross sections for para- $H_2$  at low energies. These effects are very sensitive to the details of the PES and are less prominent for collisions with ortho- $H_2$ . The enhanced resonances for para- $H_2$  are due to the limited range of orbital l values as  $j_{12} = j_1$  compared to  $j_{12} = j_1 - 1$ ,  $j_1$ ,  $j_1 + 1$  for ortho- $H_2$ . Thus, there

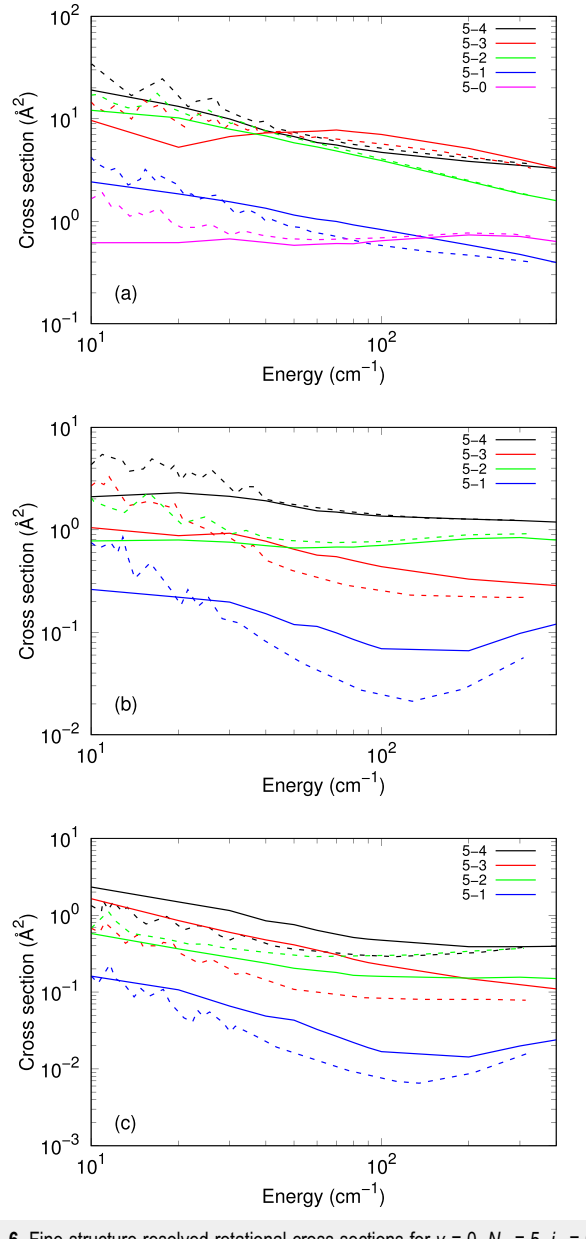


**FIG. 6.** Fine-structure resolved rotational cross sections for v = 0,  $N_1 = 5$ ,  $j_1 = 6$ , and  $N_1' = 0$ –4 induced by collisions with para-H<sub>2</sub>. Results using the 5D-CS approximation (solid lines) are compared to 2D-CC results by Lique *et al.*<sup>17</sup> (dashed lines). Panels (a)–(c) correspond to transitions  $F_1 \to F_1$ ,  $F_1 \to F_2$ , and  $F_1 \to F_3$ , respectively.

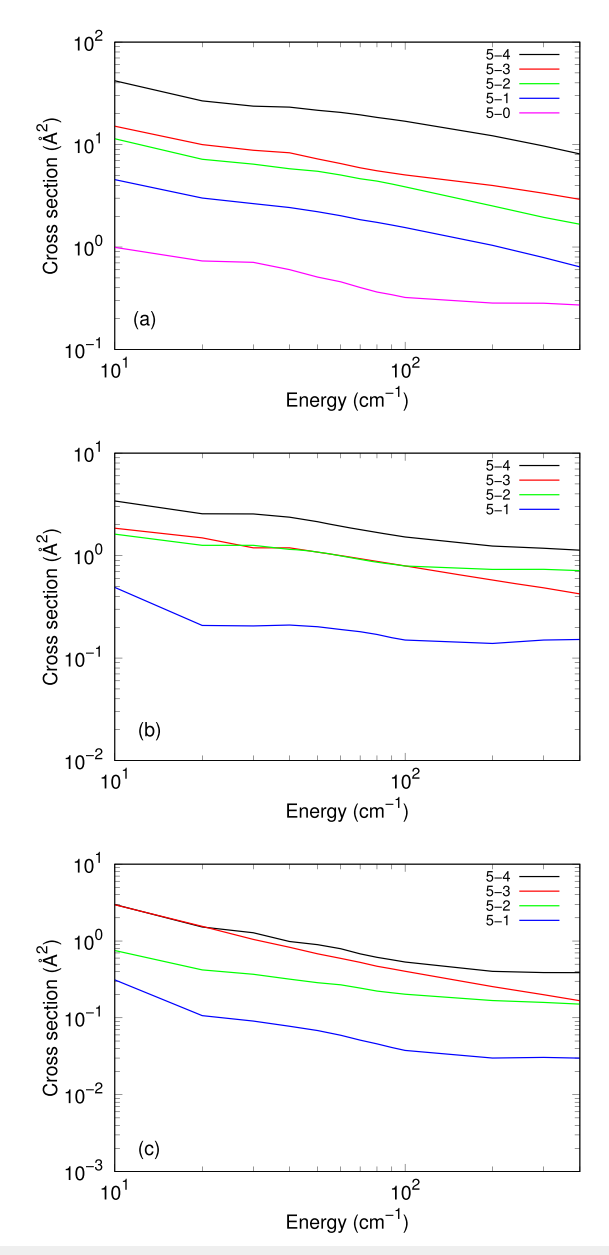


**FIG. 7.** Fine-structure resolved rotational cross sections for v = 0,  $N_1 = 5$ ,  $j_1 = 6$ , and  $N'_1 = 0$ -4 induced by collisions with ortho-H<sub>2</sub>. The 5D-CS results are plotted as in Fig. 6; however, there are no existing data in the literature to compare with.

is greater averaging of different l-contributions at low energies for ortho- $H_2$  than para- $H_2$ , leading to smoother features for ortho- $H_2$ . The 5D-CS calculations cannot provide an accurate description of resonances, so the coarse energy grid simply passes over them with a smooth curve.

Figure 4 shows rate coefficients for the transitions shown in Fig. 3 for a Maxwellian velocity distribution; the CS rate coefficients were computed using cross sections for collision energies ranging from 1 cm<sup>-1</sup> to 10 000 cm<sup>-1</sup>, while the CC rate coefficients were computed using energies from 1 cm<sup>-1</sup> to 3000 cm<sup>-1</sup>. Therefore, we compare the rate coefficients over the temperature range 10 K  $\leq$  T  $\leq$  600 K. The CC and CS results show the same main features and agree to within 25%.

Figure 5 compares cross sections for vibrational deexcitation from SO(1,5) in collisions with ortho- and para-H<sub>2</sub>. Panels (a) and (b) show the comparison as a function of collision energy for selected final states. The magnitude of these cross sections is much smaller than for pure rotational transitions, so any discrepancies in the approximations tend to get magnified. Nevertheless, the 6D-CC and 5D-CS cross sections exhibit the same qualitative behavior, with the 6D-CC cross sections consistently larger than the 5D-CS cross sections; this may be due to neglected coupling of orbital angular momentum for which  $l < \bar{l}$ . The 5D-CS cross sections for paraand ortho-H<sub>2</sub> depict nearly identical behavior in panels (a) and (b), which again is presumably due to the  $\bar{l} \equiv J$  approximation. Panel (c) shows cross sections for transitions from SO(1, 5) to SO(0,  $j_1'$ ) induced by para- $H_2$  at three collision energies; near  $j_1' = 5$ , there are interference structures that are not seen in panel (d), which shows a similar comparison but with ortho-H<sub>2</sub> as the perturber. The cross sections generally exhibit the same qualitative behavior for the different symmetries, and the 6D-CC results are typically larger by a factor of 2.

#### B. Fine-structure resolved results

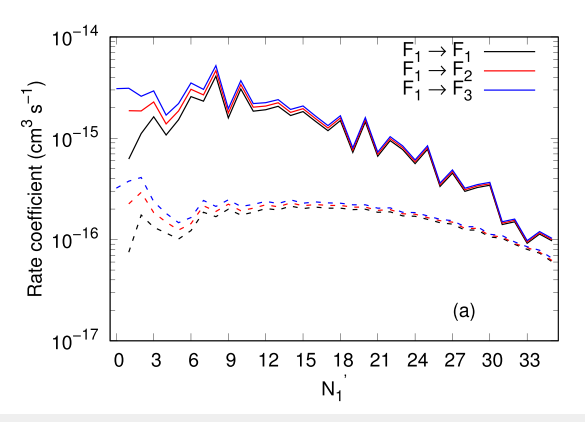
Fine-structure resolved cross sections were computed using Eqs. (8) and (10), and it was verified that the numerical results agreed in the limit that the mixing angle  $\alpha \to 0$ . The rotational quantum

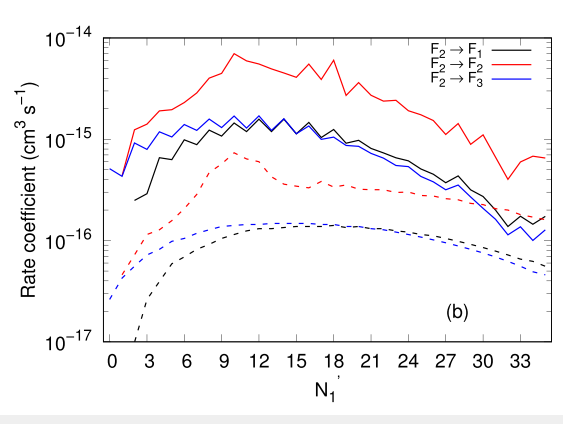
number  $N_1$  is no longer a good quantum number in the intermediate coupling scheme. Nevertheless, we follow the convention used by Lique *et al.*<sup>17</sup> and label the transitions according to the  $N_1$  value obtained in the Hund's case (b) limit. In this convention,  $N_1 = j_1 - 1$  for  $F_1$ ,  $N_1 = j_1$  for  $F_2$ , and  $N_1 = j_1 + 1$  for  $F_3$ .

Figure 6 shows cross sections for fine-structure resolved  $SO(v_1 = 0 \text{ and } N_1 = 5)$  rotational transitions due to collisions with para-H<sub>2</sub>. The 5D-CS calculations are compared with results of Lique et al. The results show similar qualitative behavior, especially at higher energies, and both calculations show the expected propensity for *F*-conserving transitions, <sup>16</sup> which correspond to  $\Delta j_1 = \Delta N_1$  collisions in the Hund's case (b) limit. It is noteworthy that the cross sections in Fig. 6 yield rate coefficients that are in better agreement than was seen in a previous comparison,<sup>23</sup> which applied a statistical average to the rate coefficients of Lique et al. 17 Nevertheless, there remain small differences that are difficult to explain due to the 5D-CS approximation in our calculations and the different PES and 2D-CC method<sup>17</sup> that was used in their calculation. In general, we find best agreement for the F-conserving transitions and poorest agreement for the relatively weak  $F_1 \rightarrow F_3$  transitions such as those shown in Fig. 6(c). It is also noteworthy that the value of the mixing angle  $\alpha$  may be tuned to bring the calculations into better agreement. While this is not a rigorous procedure, it does provide some insight into the sensitivity of the intermediate coupling scheme and shows that it is important for the weak F-changing transitions even at high values of  $j_1$  (see the supplementary material).

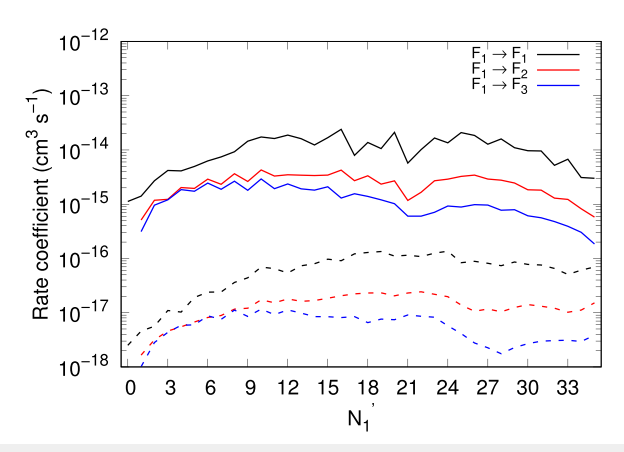
Figure 7 presents 5D-CS results similar to those shown in Fig. 6 but for collisions with ortho- $H_2$ . As expected, the cross sections show a propensity for F-conserving transitions, which resemble the spin-free results shown in Fig. 3. Whereas the cross sections for ortho- $H_2$  and para- $H_2$  are very different for F-conserving transitions, the cross sections for  $F_1 \rightarrow F_2$  and  $F_1 \rightarrow F_3$  are qualitatively similar, with the ortho- $H_2$  results generally a bit larger than those of para- $H_2$ .

Figure 8 compares the 5D-CS fine-structure resolved rate coefficients for rovibrational transitions with those calculated by Lique  $et\ al.^{19}$  using the mass-scaled results from SO-He. The perturber in both panels is para-H<sub>2</sub> for the 5D-CS calculations. Panel (a)





**FIG. 8.** Fine-structure resolved rate coefficients at T = 500 K following vibrational relaxation from  $v_1 = 1$  to 0. The dashed lines correspond to mass-scaled results from SO–He calculated by Lique *et al.*, <sup>19</sup> while the solid lines show rate coefficients found by using the 5D-CS approximation. Panel (a) shows results for transitions from SO( $v_1 = 1$ ,  $N_1 = 0$ ,  $j_1 = 1$ ), while panel (b) shows a similar plot but for SO(1, 10, 10).



**FIG. 9.** Fine-structure resolved rate coefficients at T = 500 K calculated by using the 5D-CS approximation. The vibrational de-excitation transitions shown are from SO( $v_1 = 2$ ,  $N_1 = 10$ ,  $j_1 = 11$ ) to  $v_1' = 1$  (solid lines) or  $v_1' = 0$  (dashed lines) and  $N_1' = 0$ –36.

compares the rate coefficients for transitions from  $SO(\nu_1=1,N_1=0,j_1=1)$  to  $SO(0,N_1')$  for T=500 K. Panel (b) shows a similar comparison, but for SO(1,10,10). Both calculations show the expected propensity for  $\Delta j_1=\Delta N_1$  with a marked increase at higher rotational levels. The present results are larger by about an order of magnitude and exhibit interference structures that are not seen in the mass-scaled SO–He results. These differences are presumably due to the deeper global minimum for the SO–H<sub>2</sub> PES<sup>23</sup> as compared to the SO–He PES<sup>19</sup> (158 cm<sup>-1</sup> vs 35 cm<sup>-1</sup>) and deficiencies in the mass-scaling approach. The present results show that reduced mass-scaling estimates of rate coefficients using He collider data provide a poor approximation for vibrationally inelastic collisions.

Figure 9 presents fine-structure resolved rate coefficients for transitions from  $v_1 = 2$  to  $v_1' = 0$ , 1 induced by para-H<sub>2</sub>. For such higher vibrational levels, there are no available data for comparison. Rate coefficients at T = 500 K are shown for transitions from  $SO(v_1 = 2, N_1 = 10)$  to  $SO(0, N_1')$ . The rate coefficients for  $\Delta v_1 = -1$  are about two orders of magnitude larger than those for  $\Delta v_1 = -2$  and in both cases show the expected propensity for  $\Delta j_1 = \Delta N_1$ . The results for ortho-H<sub>2</sub> are quite similar.

#### **IV. CONCLUSIONS**

Accurate rate coefficients for SO colliding with  $H_2$  are of astrophysical importance, and open questions remain in understanding environments such as protoplanetary disks where SO is present. <sup>10,11</sup> This work has presented spin-free and spin-rotation coupled results for SO in its ground state,  $SO(X^3\Sigma^-)$ , for both para- and ortho- $H_2$  perturbers restricted to their lowest two rotational levels. These calculations were performed within the 5D-CS approximation, which has been shown to be a reliable decoupling approximation that can be used when the CC calculations are intractably large. The 5D-CS results were within 30% of the available 6D-CC results. <sup>23</sup> A recent study has shown that it may be possible to further improve the 5D-CS results using machine-learning. <sup>42</sup>

The 5D-CS results presented in this article extend pure rotational fine-structure calculations to higher energies and to include

ortho- $H_2$  perturbers. Selected fine-structure resolved results were compared with those determined by Lique *et al.*<sup>17,19</sup> For  $\nu = 0$ , the two sets of calculations produce cross sections that are generally in good agreement with each other; however, we expect that the 5D-CS results may be slightly more accurate due to the improved PES and because the structure of  $H_2$  was included in the calculation.

Whereas reduced mass-scaling is often applied to estimate rate coefficients for para- $\rm H_2$  colliders from He collider data,  $^{17}$  we have found this to be a poor approximation for this collision system. The rate coefficients for vibrational quenching transitions induced by para- $\rm H_2$  are found to be larger by about an order of magnitude than those estimated by using the mass scaled results from SO–He. This difference is an example of the large error that can occur in applying mass-scaling to dynamical calculations on an incorrect PES.  $^{41}$  Due to the substantially larger quenching rate coefficients, we recommend the present results be included in the BASECOL database, and any astrophysical model that is sensitive to these rates should be re-evaluated.

Future observations with the James Webb Space Telescope (JWST) can probe vibrational SO transitions and may provide unique insights into a variety of astrophysics sources. In particular, the SO N, j=8, 9-7, 8 rotational line was used by the Atacama Large Millimeter/submillimeter Array (ALMA) to map a possible magnetohydrodynamic disk wind around a jet from a protoplanetary disk. The collisional data provided here will find important applications to JWST observations of such objects.

#### SUPPLEMENTARY MATERIAL

See the supplementary material for data and additional figures.

#### **ACKNOWLEDGMENTS**

The authors dedicate this article to Kate Kirby for her many seminal contributions in chemical physics and applications in astrophysics and for her outstanding service to all fields of physics. We thank N. Balakrishnan for a careful reading of this manuscript and helpful comments. This work was supported by the NASA (Grant No. NNX16AF09G) and the NSF (Grant No. PHY-1806180).

### APPENDIX: 5D-CS T-MATRIX ELEMENTS IN INTERMEDIATE COUPLING SCHEME

To find the mixing angle  $\alpha$ , we diagonalize the SO Hamiltonian in the Hund's case (b) basis set. The Hamiltonian is given by

$$\hat{H} = -\frac{\hbar^2}{2\mu} \frac{\partial^2}{\partial r^2} + B\hat{N}^2 + \mu \hat{N} \cdot \hat{S} + \frac{2\lambda}{3} (3\hat{S}_{\xi}^2 - \hat{S}^2),$$

where B is the rotational constant,  $\mu$  is the spin-rotation coupling constant, and  $\lambda$  is the spin-spin coupling constant. The wave function for the Hamiltonian has an angular part  $|(NS)jm_j\rangle$  and a vibrational part,  $\langle r|v\rangle = \chi_{vj}(r)$ . The vibrational part will introduce a diagonal term  $-\frac{\hbar^2}{2\mu}\langle v|\frac{\partial^2}{\partial r^2}|v\rangle$  into the Hamiltonian matrix. This diagonal term will be constant for fixed v and j, so it will not affect the eigenvectors to be determined in the next part and may be ignored.

The matrix elements of the Hamiltonian in the angular part of the Hund's case (b) basis set are given by

$$\begin{split} & \langle (N'S)j'm'_j | \hat{H} | (NS)jm_j \rangle = \delta_{NN'}\delta_{jj'}\delta_{m_jm'_j} \\ & \times \{BN(N+1) + (\mu/2)[j(j+1) - S(S+1) - N(N+1)]\} \\ & + \delta_{jj'}\delta_{m_jm'_j} \frac{2\lambda}{3} (-1)^{j+S} \sqrt{30(2N+1)(2N'+1)}S(S+1) \\ & \times (2S+1) \binom{N-2-N'}{0-0-0} \begin{cases} S-S-1 \\ 2-1-S \end{cases} \binom{j'-N'-S}{2-S-N}. \end{split}$$

By diagonalizing the  $2 \times 2$  Hamiltonian matrix defined by the above equation, we can find the mixing angle for each pair  $(\nu, j)$ . Our calculation used the experimental values of  $B_e$ ,  $\mu_e$ , and  $\lambda_e$  from the work of Bogey *et al.*<sup>31</sup> Figure 10 shows the cosine of the calculated mixing angle for  $\nu = 0$ –2 as a function of j. For  $j \ge 5$ , the mixing angle is small enough that a Hund's case (b) coupling scheme is appropriate to within 5%.

The T-matrix elements in the intermediate coupling scheme are given by

$$T^{J}_{F_{i}jl;F'_{i}j'l'} = \sum_{NN'} C^{j}_{NF_{i}} C^{j'}_{N'F'_{i}} T^{J}_{Njl;N'j'l'},$$

where the coefficients  $C^j_{NF_i}$  depend on the mixing angle  $\alpha$ . From these T-matrix elements, one can construct the cross sections

$$\sigma_{F,j \to F'_i j'} = \frac{\pi}{(2j+1)k_{F,j}^2} \sum_{J|J'} (2J+1) \left| T_{F,jJ;F'_i j'J'}^J \right|^2. \tag{A1}$$

Using the transformation<sup>28</sup>

$$\begin{split} T^{J}_{Njl;N'j'l'} &= \delta_{SS'} i^{l+l'-2\bar{l}} \sum_{m_1 m_2 \; \mu} (-1)^{l+l'} \sqrt{[jlj'l']} \\ &\times \begin{pmatrix} l & J & j \\ 0 & -\mu & \mu \end{pmatrix} \begin{pmatrix} S & N & j \\ -m_1 - \mu & m_1 & \mu \end{pmatrix} \\ &\times \begin{pmatrix} l' & J & j' \\ 0 & -\mu & \mu \end{pmatrix} \begin{pmatrix} S & N & j' \\ -m_1 - \mu & m_1 & \mu \end{pmatrix} T^{\bar{l}m_1 m_2}_{N;N'} \;, \end{split}$$

with  $[j] \equiv 2j + 1$ , one can obtain the desired cross section (10).

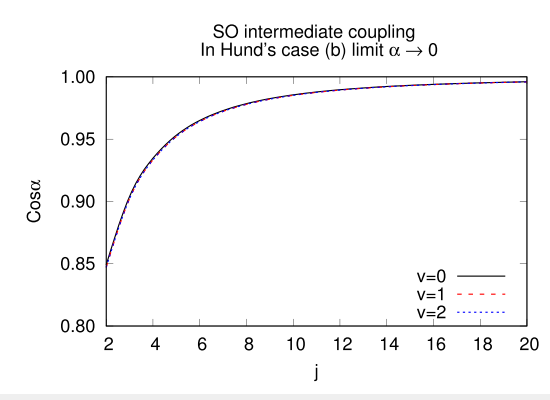


**FIG. 10.** Cosine of the mixing angle  $\alpha$  calculated by diagonalizing the SO Hamiltonian using spectroscopic constants from the work of Bodev *et al.*<sup>31</sup>

#### **DATA AVAILABILITY**

The data that support the findings of this study are available within the article and its supplementary material.

#### **REFERENCES**

<sup>1</sup>C. A. Gottlieb and J. A. Ball, "Interstellar sulfur monoxide," Astrophys. J. 184, L59 (1973).

<sup>2</sup>G. B. Esplugues, B. Tercero, J. Cernicharo, J. R. Goicoechea, A. Palau, N. Marcelino, and T. A. Bell, "A line confusion-limited millimeter survey of orion KL: III. Sulfur oxide species," Astron. Astrophys. **556**, A143 (2013).

<sup>3</sup>O. E. H. Rydbeck, A. Hjalmarson, G. Rydbeck, J. Ellder, E. Kollberg, and W. M. Irvine, "Observations of SO in dark and molecular clouds," Astrophys. J. 235, L171 (1980).

<sup>4</sup>D. A. Swade, "The physics and chemistry of the L134N molecular core," Astrophys. J. **345**, 828 (1989).

<sup>5</sup>D. A. Neufeld, B. Godard, M. Gerin, G. Pineau des Forêts, C. Bernier, E. Falgarone, U. U. Graf, R. Güsten, E. Herbst, P. Lesaffre, P. Schilke, P. Sonnentrucker, and H. Wiesemeyer, "Sulphur-bearing molecules in diffuse molecular clouds: New results from SOFIA/GREAT and the IRAM 30m telescope," Astron. Astrophys. 577, A49 (2015).

<sup>6</sup> A. E. Higuchi, J. O. Chibueze, A. Habe, K. Takahira, and S. Takano, "ALMA view of G0.253+0.016: Can cloud-cloud collision form the cloud?," Astron. J. **147**, 141 (2014).

<sup>7</sup>N. Sakai, T. Sakai, T. Hirota, Y. Watanabe, C. Ceccarelli, C. Kahane, S. Bottinelli, E. Caux, K. Demyk, C. Vastel, A. Coutens, V. Taquet, N. Ohashi, S. Takakuwa, H.-W. Yen, Y. Aikawa, and S. Yamamoto, "Change in the chemical composition of infalling gas forming a disk around a protostar," Nature 507, 78 (2014).

<sup>8</sup>L. V. Prieto, C. S. Contreras, J. Cernicharo, M. Agundez, G. Quintana-Lacaci, V. Bujarrabal, J. Alcolea, C. Balanca, F. Herpin, K. M. Menten, and F. Wyrowski, "The millimeter IRAM-30m line survey toward IK Tauri," *Astron. Astrophys.* **597**, A25 (2017).

<sup>9</sup>F. Herpin, M. Marseille, V. Wakelam, S. Bontemps, and D. C. Lis, "S-bearing molecules in massive dense cores," Astron. Astrophys. **504**, 853 (2009).

 $^{10}$ S. Pacheco-Vasquez, A. Fuente, C. Baruteau, O. Berne, M. Agundez, R. Neri, J. R. Goicoechea, J. Cernicharo, and R. Bachiller, "High spatial resolution imaging of SO and  $\rm H_2CO$  in AB Auriga: The first SO image in a transitional disk," Astron. Astrophys. **589**, A60 (2016).

<sup>11</sup> A. S. Booth, C. Walsh, M. Kama, R. A. Loomis, L. T. Maud, and A. Juhász, "Sulphur monoxide exposes a potential molecular disk wind from planet-hosting disk around HD 100546," Astron. Astrophys. 611, A16 (2018).

<sup>12</sup>E. Roueff and F. Lique, "Molecular excitation in the interstellar medium: Recent advances in collisional, radiative, and chemical processes," Chem. Rev. 113, 8906 (2013).

<sup>13</sup> J. H. Black, Astrochemistry: From Molecular Clouds to Planetary Systems (Astronomical Society of the Pacific, 2000), p. 81, IAU Symposium, No. 197.

<sup>14</sup>F. F. S. van der Tak, *Massive Star Birth* (University Press, Cambridge, 2005), p. 70, IAU Symposium, No. 227.

<sup>15</sup>F. F. S. van der Tak, J. H. Black, F. L. Schöier, D. J. Jansen, and E. F. van Dishoeck, "A computer program for fast non-LTE analysis of interstellar line spectra with diagnostic plots to interpret observed line intensity ratios," Astron. Astrophys. 468, 627 (2007).

<sup>16</sup>S. Green, "Collisional excitation of interstellar sulfur monoxide," Astrophys. J. 434, 188 (1994).

 $^{17}$ F. Lique, M.-L. Senent, A. Spielfiedel, and N. Feautrier, "Rotationally inelastic collisions of SO( $X^3$ Σ $^-$ ) with H $_2$ : Potential energy surface and rate coefficients for excitation by para-H $_2$  at low temperature," J. Chem. Phys. **126**, 164312 (2007).

<sup>18</sup>M. L. Dubernet *et al.*, "BASECOL2012: A collisional database repository and web service within virtual atomic and molecular data center (VAMDC)," Astron. Astrophys. 553, A50 (2013).

<sup>19</sup> F. Lique, A. Spielfiedel, G. Dhont, and N. Feautrier, "Ro-vibrational excitation of the SO molecule by collision with the He atom," Astron. Astrophys. 458, 331 (2006).

- <sup>20</sup> F. Lique, A. Spielfiedel, M.-L. Dubernet, and N. Feautrier, "Rotational excitation of sulfur monoxide by collisions with helium at low temperature," J. Chem. Phys. 123, 134316 (2005).
- <sup>21</sup> F. Lique, S. Spielfiedel, and N. Feautrier, "Rotational excitation of sulfur monoxide in collision with helium at high temperature," Astron. Astrophys. 450, 399 (2006).
- <sup>22</sup>F. Lique, J. Cernicharo, and P. Cox, "The excitation of SO in cold molecular clouds: TMC-1," Astrophys. J. 653, 1342 (2006).
- <sup>23</sup>B. Yang, P. Zhang, C. Qu, P. C. Stancil, J. M. Bowman, N. Balakrishnan, and R. C. Forrey, "Full-dimensional quantum dynamics of  $SO(X^3 \Sigma^-)$  in collisions with  $H_2$ ," Chem. Phys. **532**, 110695 (2020).
- <sup>24</sup>R. C. Forrey, B. H. Yang, P. C. Stancil, and N. Balakrishnan, "Mutual vibrational quenching in CO+H<sub>2</sub> collisions," Chem. Phys. 462, 71 (2015).
   <sup>25</sup>B. Yang, P. Zhang, C. Qu, X. H. Wang, P. C. Stancil, J. M. Bowman, N. Balakrish-
- <sup>25</sup>B. Yang, P. Zhang, C. Qu, X. H. Wang, P. C. Stancil, J. M. Bowman, N. Balakrishnan, B. M. McLaughlin, and R. C. Forrey, "Full-dimensional quantum dynamics of SiO in collision with H<sub>2</sub>," J. Phys. Chem. A **122**, 1511 (2018).
- <sup>26</sup>H. Burton, R. Mysliwiec, R. C. Forrey, B. H. Yang, P. C. Stancil, and N. Balakrishnan, "Fine-structure resolved rotational transitions and database for CN+H<sub>2</sub> collisions," Mol. Astrophys. 11, 23 (2018).
- <sup>27</sup> M. H. Alexander, "Rotationally inelastic collisions between a diatomic molecule in a  $^2\Sigma^+$  electronic state and a structureless target," J. Chem. Phys. **76**, 3637 (1982). <sup>28</sup> G. C. Corey and F. R. McCourt, "Inelastic differential and integral cross sections for  $^{2S+1}\Sigma$  linear molecule  $^1S$  atom scattering: The use of Hund's case (b) representation," J. Phys. Chem. **87**, 2723 (1983).
- <sup>29</sup>A. R. Offer, M. C. v. Hemert, and E. F. v. Dishoeck, "Rotationally inelastic and hyperfine resolved cross sections for OH-H<sub>2</sub> collisions. Calculations using a new *ab initio* potential surface," J. Chem. Phys. **100**, 362 (1994).
- <sup>30</sup>G. C. Corey, M. H. Alexander, and J. Schaefer, "Quantum studies of inelastic collisions of  $O_2(X^3\Sigma_g^-)$  with He: Polatization effects and collisional propensity rules," J. Chem. Phys. **85**, 2726 (1986).
- <sup>31</sup>M. Bogey, C. Demuynck, and J. L. Destombes, "Millimeter wave spectrum of SO in highly excited vibrational states: Vibrational and isotopic dependence of molecular constants," Chem. Phys. 66, 99 (1982).

- $^{32}$ D. W. Schwenke, "Calculations of rate constants for the three-body recombination of  $H_2$  in the presence of  $H_2$ ," J. Chem. Phys. **89**, 2076 (1988).
- $^{33}$ Q. Qian, C. L. Yang, F. Gao, and X. Y. Zhang, "Multi-reference configuration interaction study on analytical potential energy function and spectroscopic constants of XOn(X=S,Cl;  $n=0,\pm 1$ )," Acta Phys. Sin. **56**, 4420 (2007).
- <sup>34</sup>R. Krems, *TwoBC-Quantum Scattering Program* (University of British Columbia, Vancouver, Canada, 2006).
- <sup>35</sup>B. R. Johnson, "The multichannel log-derivative method for scattering calculations," J. Comput. Phys. 13, 445 (1973).
- <sup>36</sup>D. E. Manolopoulos, "An improved log derivative method for inelastic scattering," J. Chem. Phys. 85, 6425 (1986).
- <sup>37</sup>K. T. Lee and J. M. Bowman, "Rotational distributions from resonant and direct scattering in H+CO and tests of statistical theories," J. Chem. Phys. **86**, 215 (1987).
- <sup>38</sup>S. D. Augustin and W. H. Miller, "Classical trajectory study of rotational excitation in low energy He-CO and He-H<sub>2</sub> collisions," Chem. Phys. Lett. **28**, 149 (1974).
- <sup>39</sup>S. Chapman and S. Green, "Rotational excitation of linear molecules by collisions with atoms: Comparison of classical and quantum methods," J. Chem. Phys. **67**, 2317 (1977).
- <sup>40</sup>C. W. McCurdy and W. H. Miller, "Interference effects in rotational state distributions: Propensity and inverse propensity," J. Chem. Phys. 67, 463 (1977).
- <sup>41</sup> K. M. Walker, B. H. Yang, P. C. Stancil, N. Balakrishnan, and R. C. Forrey, "On the validity of collider-mass scaling for molecular rotational excitation," Astrophys. J. 790, 96 (2014).
- <sup>42</sup>A. Jasinski, J. Montaner, R. C. Forrey, B. H. Yang, P. C. Stancil, N. Balakrishnan, J. Dai, R. A. Vargas-Hernandez, and R. V. Krems, "Machine learning corrected quantum dynamics calculations," Phys. Rev. Res. 2, 032051(R) (2020).
- <sup>43</sup>B. Tabone, S. Cabrit, E. Bianchi, J. Ferreira, G. Pineau des Forêts, C. Codella, A. Gusdorf, F. Gueth, L. Podio, and E. Chapillon, "ALMA discovery of a rotating SO/SO<sub>2</sub> flow in HH212. A possible MHD disk wind?," Astron. Astrophys. 607, L6 (2017).